Analytical solution of a kinematic wave approximation for channel routing

P. Reggiani, E. Todini and D. Meißner

ABSTRACT

The kinematic wave approach is often used in hydrological models to describe channel and overland flow. The kinematic wave is suitable for situations where the local and convective acceleration, as well as the pressure term in the dynamic wave model is negligible with respect to the friction and body forces. This is the case when describing runoff processes in the upper parts of catchments, where slopes are generally of the order of 10^{-3}. In physical-based hydrological models, the point-scale conservation equations are integrated over model entities, such as grid pixels or control volumes. The integration leads to a set of ordinary differential governing equations, which can be solved numerically by methods such as the Runge–Kutta integrator. Here, we propose an analytical solution of a Taylor-series approximation of the kinematic wave equation, which is presented as non-linear reservoir equation. We show that the analytical solution is numerically robust and third-order accurate. It is compared with the numerical solution and the solution of the complete dynamic wave model. The analytical solution proves to be computationally better performing and more accurate than the numerical solution. The proposed analytical solution can also be generalized to situations of leaking channels.

Key words | analytical solution, channel routing, kinematic wave, representative elementary watershed model, River Mosel

P. Reggiani (corresponding author)
Deltares,
P.O. Box 177,
2600MH Delft,
The Netherlands
and
Department of Physical Geography, and
    Climatology,
RWTH Aachen University,
52056 Aachen,
Germany
E-mail: paolo.reggiani@deltares.nl

E. Todini
BiGeA, University of Bologna,
Via Zamboni 67,
40126 Bologna,
Italy

D. Meißner
Bundesanstalt für Gewässerkunde,
Am Mainzer Tor 1,
56068 Koblenz,
Germany

NOTATION

a, c, k	hydraulic geometry coefficients
A	area of reach cross section
b, f, m	hydraulic geometry exponents
g	gravity constant
n	Manning roughness
P_w	wetted perimeter of channel segment
q_{lat}	lateral inflow per unit channel length
q_{gw}	reach–groundwater exchange
Q	discharge
Q_{in}	up-stream inflow into channel segment
Q_{out}	down-stream outflow from channel segment
R_h	hydraulic radius
S_0	channel bed slope
S_f	friction slope
t	time
v	channel velocity Q/A
V	volume of channel segment
w	channel top width
x	x-coordinate along channel axis
y	channel depth coordinate
Y	channel maximum depth (Leopold & Maddock 1953)
$\overline{Y}$	channel average depth (Leopold & Maddock 1953)
$\triangle x$	channel segment length
τ	truncation error
$\xi; \zeta$	generic integration variables

INTRODUCTION

Channel, overland (Hortonian and saturation excess) and sub-surface storm flow are important runoff mechanisms that characterize the hydrological response footprint of a watershed. A comprehensive hydrological model should include

separate descriptions of these mechanisms. Surface and subsurface runoff are typical processes that are included in most models in the literature. Channel flow can be simulated by combining a hydrological model with an external dynamic wave model, for which the hydrological model provides the lateral inflow. The choice of modelling the channel separately is motivated by the potential need to describe flow propagation via a complete dynamic wave model (Chow 1968) instead of using simpler approaches. A full dynamic representation becomes necessary when modelling river flow over very mild slopes (of the order of 0.5×10^{-3} or milder), where storage effects cannot be neglected and surface gradients as well as inertial terms (local and convective acceleration) become important. A commonly used alternative to the dynamic wave model is the variable-parameter Muskingum–Cunge (MC) routing method. Cunge (1969) modified the original fixed-parameter linear Muskingum approach introduced by McCarthy (1940), which he interpreted as a first-order kinematic approximation of a diffusion wave model. Cunge converted it into a parabolic model by enabling variable parameters in time according to a suitable estimation of the parameter values that matches the physical to the numerical diffusion. Todini (2007) revised and generalized the variable-parameter MC method, thus addressing situations in which the original scheme is not mass conservative (Ponce & Yevjevich 1978; Tang *et al.* 1999). Notably, the modified MC method can now adequately capture non-linear effects of the dynamic wave such as the hysteresis loop of the stage–discharge curve.

In watershed hydrology, the use of complex physical-based routing is often replaced by much simpler analogies, which still provide accurate flow descriptions in situations where second-order effects are negligible. This choice is mainly motivated by the comparatively modest input data requirement by the latter and the option not to use detailed channel geometries, which are required in the complete dynamic wave model, but which in practice are frequently coarsely described or not available (e.g. in ungauged basins). Examples include several simplifications of the dynamic wave model, which yields a hyperbolic differential equation (Henderson 1966). Otherwise, flood propagation can be studied by a diffusion wave analogy formulated in terms of a parabolic differential equation, which is derived from the dynamic wave model through linearization and negligence of acceleration terms (Hayami 1951; Lighthill & Whitham 1955; Dooge 1973). The parameters for the linear routing schemes can be derived either by direct physical interpretation or by matching hydrodynamic patterns (Kundzewicz 1985). Flow routing in hydrology can also be set aside completely and replaced by a cascade of linear reservoirs (Nash 1957), in which the outflow of a storage element is assumed to be a linear function of storage, allowing for an analytical solution. Kalinin & Miljukov (1957) demonstrated that a river channel can be modelled as a succession of linear reaches of characteristic length, which, similar to the Nash cascade model, leads to a gamma function response, whose parameters can be derived from the physical properties instead of being estimated from input–output data as in the Nash modelling approach (Kalinin & Miljukov 1957; Dooge 1973; Strupczewski & Kundzewicz 1979).

Similarly, the use of the mass balance equation, where closure schemes for fluxes across storage elements boundaries (channel cross sections) are expressed in terms of power laws, can also be used instead of linear relationships. The model parameters are introduced ad hoc, and are usually not interpretable in terms of measurable quantities, such as channel slope and geometry or bed friction, leaving the effects of gravity unaccounted for. The power law parameters need to be determined on the basis of calibration, whereby historical time series of observed discharges are needed. Examples include the HBV (Bergström 1995), the Sacramento (Crawford & Linsley 1966) or the Xinanjiang (Zhao 1992) models. Important drawbacks are that readily available information such as digital terrain elevation remains unused, and an application to ungauged basins is impossible in the absence of historical observations.

Owing to the rapid progress in space-borne data acquisition, recent research is oriented towards the development of process-based hydrological models, in which the physical principles governing the flow are explicitly included. The underlying formulations start from the point-scale conservation equations for mass and momentum and integrate these up to spatial scales, which are meaningful for hydrological applications. The spatial domain over which the point-scale equations are integrated differs between approaches. It can either consist of elements of a square lattice by a landscape discretization into a pixel grid, or of more general shapes, such as generic control volumes defined on the basis of a topographically driven subdivision. The

topographic kinematic approximation and integration model (Liu & Todini 2002, 2004; Liu *et al.* 2005) introduces a series of conservation equations at the spatial scale of a pixel, whereas the representative elementary watershed (REW) formulation (Reggiani *et al.* 1998; Reggiani & Rientjes 2005) defines irregularly shaped control volumes for different types of flows and independently of spatial scale.

The integration of the point-scale conservation law of mass leads to a transformation of local gradients into fluxes across the boundaries of the storage elements. The fluxes need to be closed by appropriately combining mass and momentum conservation. The combination yields to a non-linear ordinary differential equation (ODE) for a reach segment, whose analytical solution is only available for specific values of the exponent (as, for instance, when the exponent equals 1, namely in the linear reservoir case), but not in general. Therefore, this ODE can be solved analytically with linear approximations (Ostrowski 1992) or numerically with methods such as the Runge–Kutta (RK) integrator (Reggiani *et al.* 2001; Todini & Ciarapica 2001). In the interest of numerical efficiency, we demonstrate that under restrictive assumptions, such as time-invariant (averaged) lateral inflow into a channel segment over an integration timestep, and based on an approximation of the non-linear reservoir equation introduced by Liu & Todini (2002), it is possible to find an analytical solution that is equivalent to the non-linear kinematic wave model (Liu & Todini 2004). Note that the resulting non-linear reservoir equation model highly differs from the previously cited approaches, such as the Nash reservoirs cascade (Nash 1957) or the Kalinin & Miljukov (1957) approach, in that it is the result of the discretization at the scale of the reach of the non-linear kinematic model, as opposed to the mentioned approaches, which are discretizations of the linear kinematic model. The approximation of the original equation is obtained by means of a second-order polynomial. Here, we revisit the theory and perform an error analysis of the approximated solution. Moreover, we extend the theory to include analytical solutions for the case of channel–aquifer exchange. The implementation of the analytical solution proves to be computationally efficient with potential for a wide range of applications in hydrological models. The analytical solution should however be used by acknowledging the restrictive assumptions of the kinematic wave model.

The paper is structured as follows: the background section revisits the theory, then the analytical solution is presented, while the section on channel geometry describes the hydraulic representation of the cross sections. The section on numerical analysis examines the analytical solution, the sections on applications and simulations describe the model implementation, and then the results are discussed.

BACKGROUND

The dynamic wave model, known as the Saint-Venant (SV) equations, is derived by integrating the point-scale conservation equations of mass and momentum over the cross section of a channel slab of infinitesimal thickness. In this process, the SV assumptions (Chow 1968) are applied: (i) hydrostatic pressure, (ii) uni-dimensional flow, (iii) incompressible fluid, (iv) depth and velocity vary only in the longitudinal direction, (v) steady-state flow resistance, and (vi) small bed slope with a fixed channel bed. The mass conservation equation for the infinitesimal slab is:

$$\frac{\partial A}{\partial t} + \frac{\partial Q}{\partial x} = q_{\text{lat}} + q_{\text{gw}} \qquad (1)$$

where $Q(x, t)$ is the discharge and $A(x, t)$ is the cross-sectional area at location x and time t. The terms $q_{\text{lat}}(x, t)$ and $q_{\text{gw}}(x, t)$ defined per unit channel length are, respectively, the lateral inflow and a recharge/loss term representing the interaction between the channel and the groundwater system. The latter term is positive in the case of groundwater discharge into the reach or negative in the case of groundwater recharge from the channel. Direct input through precipitation and evaporation across the top surface are omitted. The momentum conservation equation for the infinitesimal slab reads:

$$\frac{\partial Q}{\partial t} + \frac{\partial (Q^2/A)}{\partial x} + gA\left(\frac{\partial y}{\partial x} - S_0\right) + gAS_{\text{f}} = 0 \qquad (2)$$

In the kinematic wave model, the inertial term (first term on the left-hand side (l.h.s.)), the convective acceleration term (second term on the l.h.s.) and the pressure term ($\partial y/\partial x \approx 0$) are neglected, while the slope of the energy

line S_f is derived from Manning's formula. Consequently, Equation (2) reduces to a steady-state flow equation:

$$\frac{Q}{A} = \frac{1}{n} R_h^{2/3} S_f^{1/2} \tag{3}$$

where n is the Manning coefficient and R_h is the hydraulic radius. Integration of Equation (1) over a channel segment of length Δx yields a time-dependent expression:

$$\frac{dV(t)}{dt} + (Q_{out} - Q_{in}) = \int_{\Delta x} (q_{lat} + q_{gw}) dx \tag{4}$$

The inflow Q_{in} is provided by the outflow of the up-stream reaches meeting at the segment's inflow section. Under the kinematic wave model assumption, the outflow Q_{out} is provided by Equation (3). By recalling that the hydraulic radius is defined as $R_h = A/P_w$, where P_w is the wetted perimeter, and for q_{lat} and q_{gw} constant over Δx, we obtain the non-linear reservoir equation for a channel segment of length Δx:

$$\frac{dV(t)}{dt} = Q_{in} + (q_{lat} + q_{gw})\Delta x - \frac{S_f^{1/2}}{n} \frac{P_w}{(P_w \Delta x)^{5/3}} V(t)^{5/3} \tag{5}$$

whereby Q_{in}, P_w, q_{lat} and q_{gw} can still vary in time. Next, we proceed to deriving an analytical solution of Equation (5) for different values of $Q_{in} + (q_{lat} + q_{gw}) \Delta x$ corresponding to net recharge or discharge situations of the channel segment. In particular the term q_{gw} can switch sign depending on leakage from the channel towards the groundwater or vice versa.

ANALYTICAL SOLUTION

In the quest for an analytical solution for Equation (5), we rewrite the expression by assuming that the term $\mathcal{A} = Q_{in} + (q_{lat} + q_{gw}) \Delta x$ and $\mathcal{B} = S_f^{1/2} P_w/[n(P_w \Delta x)^{5/3}]$ remains constant over a typical integration interval Δt:

$$\frac{dV}{dt} = \mathcal{A} - \mathcal{B} \cdot V^\gamma \tag{6}$$

Generically, an analytical solution for Equation (6) is not available. Analytical solutions for Equation (6) are only known in a limited number of cases, as

for $\mathcal{A} = 0$; $\mathcal{B} = 0$; $\gamma = 0$; $\gamma = 1$; $\gamma = 2$ shown in Appendix A (available online at http://www.iwaponline.com/nh/045/157. pdf). In the case of kinematic flood routing, where $\gamma = 5/3$ and $\mathcal{A} \neq 0$, we propose a Taylor-series approximation of V^γ described later. In principle, a least-squares polynomial could also be used in finding an analytical solution; however, this approach bears the potential for numerical drawbacks, and therefore we refrain from pursuing it further.

Taylor-series approximation

In searching for an analytical solution, the second right-hand side (r.h.s.) term in Equation (6) is expanded as a second-order Taylor polynomial around the centre point of the volume between time t and $t + \Delta t$, denoted by $V_{\frac{\Delta t}{2}} = V_{t^-} + (\mathcal{A} - \mathcal{B} V_t^\gamma) \Delta t/2$:

$$\mathcal{A} - \mathcal{B} \cdot V^\gamma = f|_{\frac{\Delta t}{2}} + \frac{f'|_{\frac{\Delta t}{2}}}{1!} (V - V_{\frac{\Delta t}{2}}) + \frac{f''|_{\frac{\Delta t}{2}}}{2!} (V - V_{\frac{\Delta t}{2}})^2 + O(\Delta V^3) \tag{7}$$

with $\Delta V = V - V_{\frac{\Delta t}{2}}$, and the first- and second-order derivatives are defined as follows:

$$\begin{aligned} f|_{\frac{\Delta t}{2}} &= \mathcal{A} - \mathcal{B} V_{\frac{\Delta t}{2}}^\gamma \\ f'|_{\frac{\Delta t}{2}} &= -\mathcal{B} \gamma V_{\frac{\Delta t}{2}}^{\gamma-1} \\ f''|_{\frac{\Delta t}{2}} &= -\mathcal{B} \gamma(\gamma-1) V_{\frac{\Delta t}{2}}^{\gamma-2} \end{aligned} \tag{8}$$

After insertion and rearrangements, one can state the l.h.s. in Equation (6) as:

$$\frac{dV}{dt} = \lim_{\Delta t \to 0} \frac{\Delta V}{\Delta t} = \left[\hat{A} (V^2 + \hat{B} V + \hat{C}) + O(\Delta V^3) \right] \tag{9}$$

The Taylor-series polynomial coefficients are defined as:

$$\begin{aligned} \hat{A} &= -\frac{1}{2} B \gamma(\gamma-1) V_{\frac{\Delta t}{2}}^{\gamma-2} \\ \hat{B} &= -2 \frac{(\gamma-2)}{(\gamma-1)} V_{\frac{\Delta t}{2}} \\ \hat{C} &= \frac{\mathcal{A}}{\hat{A}} + \frac{(\gamma-2)}{\gamma} V_{\frac{\Delta t}{2}}^2 \end{aligned} \tag{10}$$

Through the Taylor-series expansion, V^γ in Equation (6) has effectively been substituted by a second-order polynomial. At this stage, we can perform an integration for cases with $\mathcal{A} \neq 0$, obtaining respective solutions in closed form as shown next. Two cases need to be distinguished depending on the channel inflow and outflow terms, influencing the sign and magnitude of $\mathcal{A}$ and $\mathcal{C}$:

Case 1 : $\mathcal{A} \neq 0, \ \hat{B}^2 - 4\hat{C} \geq 0$

After we neglect the error term $O(\Delta V^3)$, an approximated integral solution can be found analytically by variable separation and integration of Equation (9):

$$\int \frac{1}{V^2 + \hat{B}\,V + \hat{C}} \, \mathrm{d}V = \hat{A} \int \mathrm{d}t + \text{const.} \tag{11}$$

for which a primitive is available in closed form. The second-order polynomial at the denominator can be factorized:

$$\frac{1}{V^2 + \hat{B}\,V + \hat{C}} = \frac{1}{(V - p_1)\,(V - p_2)} \tag{12}$$

where p_1 and p_2 are real roots of the second-order polynomial:

$$p_1 = \frac{-\hat{B} + \sqrt{\hat{B}^2 - 4\hat{C}}}{2} \geq 0 \tag{13}$$

$$p_2 = \frac{-\hat{B} - \sqrt{\hat{B}^2 - 4\hat{C}}}{2} \geq 0 \tag{14}$$

Substitution into Equation (11) and integration finally yield the following primitive:

$$\hat{A}\,\Delta t = \frac{1}{(p_1 - p_2)} \ln\left[\frac{(V - p_1)}{(V - p_2)}\right] + \text{const.} \tag{15}$$

which can be re-arranged and evaluated between $[t, \Delta t]$ and $[V_t, V_{t+\Delta t}]$ as follows:

$$\left[\frac{(V - p_1)}{(V - p_2)}\right]_{V_t}^{V_{t+\Delta t}} = e^{\hat{A}\,(p_1 - p_2)\,\Delta t} \tag{16}$$

After setting:

$$e_t = \left[\frac{(V_t - p_1)}{(V_t - p_2)}\right] \cdot e^{\hat{A}\,(p_1 - p_2)\,\Delta t} \tag{17}$$

the analytical solution for $V_{t+\Delta t}$ becomes:

$$V_{t+\Delta t} = \frac{p_1 - p_2\,e_t}{(1 - e_t)} \tag{18}$$

Case 2 : $\mathcal{A} \neq 0, \ \hat{B}^2 - 4\hat{C} < 0$

For negative values of $\hat{B}^2 - 4\hat{C}$, a different integration approach needs to be adopted. First, we complete the quadratic in the denominator in Equation (11) in such a way that we can reduce it to an integrable expression. Adding and subtracting $\frac{1}{4}\hat{B}^2$ yields:

$$\frac{1}{V^2 + \hat{B}\,V + \frac{1}{4}\hat{B}^2 - \frac{1}{4}\hat{B}^2 + \hat{C}} = \frac{1}{(V + \frac{1}{2}\hat{B})^2 - \frac{1}{4}\hat{B}^2 + \hat{C}} \tag{19}$$

After substitution into Equation (11) and by integrating the l.h.s. between V_t and $V_t + \Delta t$ and the r.h.s. between t and $t + \Delta t$, one obtains:

$$\int_{V_t}^{V_{t+\Delta t}} \frac{1}{(V + \frac{1}{2}\hat{B})^2 - \frac{1}{4}\hat{B}^2 + \hat{C}} \, \mathrm{d}V = \hat{A} \int_t^{t+\Delta t} \mathrm{d}\xi \tag{20}$$

The integral on the r.h.s. can be performed analytically leading to Δt; equally, the integral on the l.h.s can be performed by setting $\hat{D} = \hat{C} - \frac{1}{4}\hat{B}^2$ and $u = V + \frac{1}{2}\hat{B}$, which leads to:

$$\int_{V_t + \frac{1}{2}\hat{B}}^{V_{t+\Delta t} + \frac{1}{2}\hat{B}} \frac{\mathrm{d}u}{u^2 + \hat{D}} = \hat{A}\,\Delta t \tag{21}$$

The indefinite integral of $\mathrm{d}u / (u^2 + \hat{D})$ is a known form:

$$\int \frac{\mathrm{d}u}{u^2 + \hat{D}} = \hat{D}^{-1/2} \arctan\left(\frac{u}{\hat{D}^{1/2}}\right) + \text{const.} \tag{22}$$

which allows evaluation of Equation (21) as:

$$\left[\hat{D}^{-1/2} \arctan\left(\frac{u}{\hat{D}^{1/2}}\right)\right]_{V_t + \frac{1}{2}\hat{B}}^{V_{t+\Delta t} + \frac{1}{2}\hat{B}} = \hat{A}\,\Delta t \tag{23}$$

The resulting analytical solution is finally:

$$V_{t+\Delta t} = -\frac{\hat{B}}{2} + \hat{D}^{1/2} \tan\left[\arctan\left(\frac{V_t + \frac{\hat{B}}{2}}{\hat{D}^{1/2}}\right) + \hat{D}^{1/2}\,\hat{A}\,\Delta t\right] \quad (24)$$

which is defined for values of the term between square brackets $[\quad] \in \mathbb{R}\backslash\{k\pi + \frac{1}{2}\pi, k \in \mathbb{Z}\}$. In this way, the analytical solution is fully generalized for all possible values of $\hat{B}^2 - 4\hat{C}$ and $\mathcal{A} \neq 0$.

CHANNEL GEOMETRY

Solution of Equation (5) requires the knowledge of the wetted perimeter P_w. In the absence of regional data, standard assumptions such as a rectangular, semicircular, triangular or trapezoidal cross section can be adopted. If observations of stream flow and channel morphology are accessible, a regionalized approach for the estimation of channel geometry can be used (Naden *et al.* 1999). Snell & Sivapalan (1995) proposed to estimate P_w using a combination of empirical hydraulic geometry relationships by Leopold & Maddock (1953). These power laws tie the average velocity, channel top width and average depth to steady-state discharge under a gradually varying flow regime and uniform roughness. Under reasonable assumptions, these relationships can be extrapolated to non-steady situations. For a reach, the top width w, average depth $\bar{Y}$ and velocity v at a point in time (at-a-station) or along stream locations fixed in time (down-stream) can be expressed as power laws of Q:

$$\begin{aligned} w &= a\,(Q)^b \\ \bar{Y} &= c\,(Q)^f \\ v &= k\,(Q)^m \end{aligned} \quad (25)$$

where the scaling coefficients a, c and k are a combination of the at-a-station and down-stream coefficients and can vary regionally. The exponents b, f and m remain independent of space and time. The coefficients and exponents of the hydraulic geometry relationships are established on the basis of field surveys. It can be proven that the maximum

depth Y at-a-station depends on $\bar{Y}$ as follows:

$$Y = \bar{Y}(b/f + 1) \quad (26)$$

The at-a-station wetted perimeter P_w can be derived by integration over depth:

$$P_w = 2\int_0^w \int_0^Y \left[1 + \frac{1}{4}\left(\frac{d\xi}{d\zeta}\right)^2\right]^{0.5} d\zeta d\xi \quad (27)$$

where ξ and ζ are dummy variables integrated between 0 and w and 0 and Y. The integral cannot be obtained in closed form and must be evaluated numerically. Details of the channel geometry formulation can be accessed in Snell & Sivapalan (1995).

NUMERICAL ANALYSIS

Properties of the approximated solution

At this stage, it is important to perform a numerical analysis of the approximated analytical solution to verify if it is accurate, consistent, stable, convergent and conservative. We note that the analysis below is an error assessment of the integral formulation of the initial-value problem:

$$V(t) - V(t_0) = \int_{t_0}^t \frac{dV}{d\zeta}d\zeta = \int_{t_0}^t F[V(\zeta), \zeta]d\zeta \quad (28)$$

whereby the differential and the integral formulation are mutually linked via the fundamental theorem of calculus.

Accuracy and consistency

An approximate solution of a differential equation is said to be *consistent*, if the local truncation error between the approximation and the exact solution vanishes as the step-size decreases towards zero. The local truncation error at time t is expressed as the difference between the volume V_t given by the approximated solution of Equation (18) and the exact one $\tilde{V}_t$:

$$\tau_t = V_t - \tilde{V}_t \quad (29)$$

By exploiting the algebraic properties of the Landau notation $O(\,)$, which quantifies the higher order terms of the approximation, Equation (11) is restated as:

$$\int_{V_t}^{V_{t+\Delta t}} \frac{1}{V^2 + \hat{B}\,V + \hat{C}}\,dV = \hat{A}\int_t^{t+\Delta t} d\xi + O(\Delta V^4) \qquad (30)$$

By invoking the analytical expression for $V_{t+\Delta t}$ in Equation (18), the local truncation error is stated as follows:

$$\tau_{t+\Delta t} = \frac{p_1 - p_2\,e_t}{(1 - e_t)} - \tilde{V}_{t+\Delta t} = O(\Delta V^4) \qquad (31)$$

In other words, the local truncation error grows asymptotically no faster than ΔV^4. By recognizing that ΔV scales like Δt and choosing progressively smaller timesteps, the error between the exact solution and the approximated analytical solution tends towards zero with the fourth power of the stepsize. As such, the approximated solution is, by definition, *consistent*. The approximated solution is also said to be third-order *accurate*, one order below the local truncation error. The same can be shown to also hold for the solution in the form of Equation (24).

Stability

The approximate analytical solution given by Equation (18) remains defined and does not asymptotically blow up, if the denominator is different from zero, thus if $e_t \neq 1$. This condition requires foremost that (i) $p_1 \neq p_2$ and that (ii) $\hat{A} \neq 0$. Conditions (i) and (ii) are always met due to the non-zero discriminant of the quadratic polynomial and the very definition of $\hat{A}$. For the case in which $\Delta t \to 0$, it can easily be shown that $V_{t+\Delta t} \to V_t$, thus the solution continues to remain stable. By analogy, the stability of the solution (24) can be proven for all values in which it is defined.

Convergence

A numerical solution is said to be *convergent*, if the global truncation error E_n at step n tends towards zero for a decreasing timestep, thus the approximated solution converges towards the exact one over the sum of all n integration steps. Under fairly general assumptions, such as when a function is locally Lipschitz continuous, it can be proven that if the approximated solution is of order m as measured by the local

truncation error, then the global error is bounded by a multiple of Δt^m. Under the condition of local Lipschitz continuity of V_t given by Equation (18), we show in Appendix B (available online at http://www.iwaponline.com/nh/045/157.pdf) that the following relationship holds:

$$E_n \leq L\,n\,\Delta t + K\,\Delta t^m \,;\ \ m \geq 1 \qquad (32)$$

where L and K are constants. It follows that the global error is bounded and tends towards zero as $\Delta t \to 0$ and the approximated solution converges to the exact solution. A similar proof can be obtained for the solution in the form of Equation (24).

Conservation

As a corollary of the previous analysis, it follows that the method is conservative. The mass outflow from a channel reach is given by Equation (9). It is obvious that for $\Delta t \to 0$, the Taylor-series approximation of the volume derivative tends towards the exact analytical expression (6), thus ensuring conservation.

APPLICATION

Study area and hydrology

To test the analytical solution, we applied it to flood propagation in the River Mosel. The Mosel drains a 29,000 km² basin and is one of the largest tributaries to the River Rhine. The lower catchment area includes mainly Germany, with parts of the upper basin situated in France and Luxembourg. The Mosel joins the Rhine at the city of Koblenz. The long-term average flow in the Mosel at Koblenz is about 330 m³/s. Peak discharges of approximately 4,200 m³/s have been recorded, making the Mosel a significant contributor to the Rhine. Therefore, accurate flow forecasting in River Mosel is very relevant for flow prediction on the Rhine, and attracts stakeholder interest to compare computational and forecasting performance of non-linear routing methods. A drawback of using the Mosel River system for the present study is the high level of river training, as the Mosel also serves navigation and hydro-electric generation purposes. The engineering works have a severe impact on low-flow regimes, but their effect is felt more during low-flow periods and gradually disappears

during medium to high flows, where the structures are operated in such a way as to allow floods to propagate undisturbed.

The Mosel has been selected as the study system because a pre-operational forecasting system based on the REW model (Reggiani & Rientjes 2005) is currently tested at the forecasting office at the Federal Institute of Hydrology in Koblenz (BFG). Meteorological forcing data over the 16 year period 1996–2011 are available at hourly intervals, including hourly water-level observations transformed into discharges at several locations, including Cochem and Trier. These data were utilized to calibrate and validate the REW model, which is used to estimate lateral inflows into the Mosel and main tributaries. The Nash–Sutcliffe coefficient was used as a performance indicator by comparing simulated discharges against observations at Cochem and Trier for daily average flows. Channel routing is performed using the integral kinematic wave approach as stated by Equation (6). The choice of the kinematic wave is justified by the main channel bed slope, which is around 1.12×10^{-3} on average, and by the relatively low hydraulic roughness. In fact, the Mosel is known to behave as a kinematic system, by barely exhibiting any parabolic behaviour and looped stage–discharge relationships anywhere in the river, which will also become clear from the results.

The main objective here is to compare the proposed kinematic wave solution with a full dynamic wave solution in a real setting. The ODEs governing the system of non-linear reservoir equations are formulated for individual stream channel segments and are resolved analytically as well as with a fifth-order RK ODE solver (Press *et al.* 2002). The results are compared with flood propagation using the finite-difference solution of the dynamic wave model with the SV equation solver SOBEK (Stelling & Duinmeijer 2003) used operationally by the BFG. The SOBEK model contains a total of 455 high-resolution cross-section profiles. Over a length of 240 km, this corresponds to circa one profile every 500 m. The spatial resolution of the computation grid includes 726 nodes. The Manning roughness in the SOBEK model is variable, with values ranging between 0.022 and 0.025.

Stream network characteristics

The channel network was extracted from a 75×75 m digital elevation model (DEM). Different spatial resolutions of the network can be defined. If a single reach per REW is used, we obtain a network of 85 reaches, as shown in Figure 1. Alternatively a higher-resolution network with
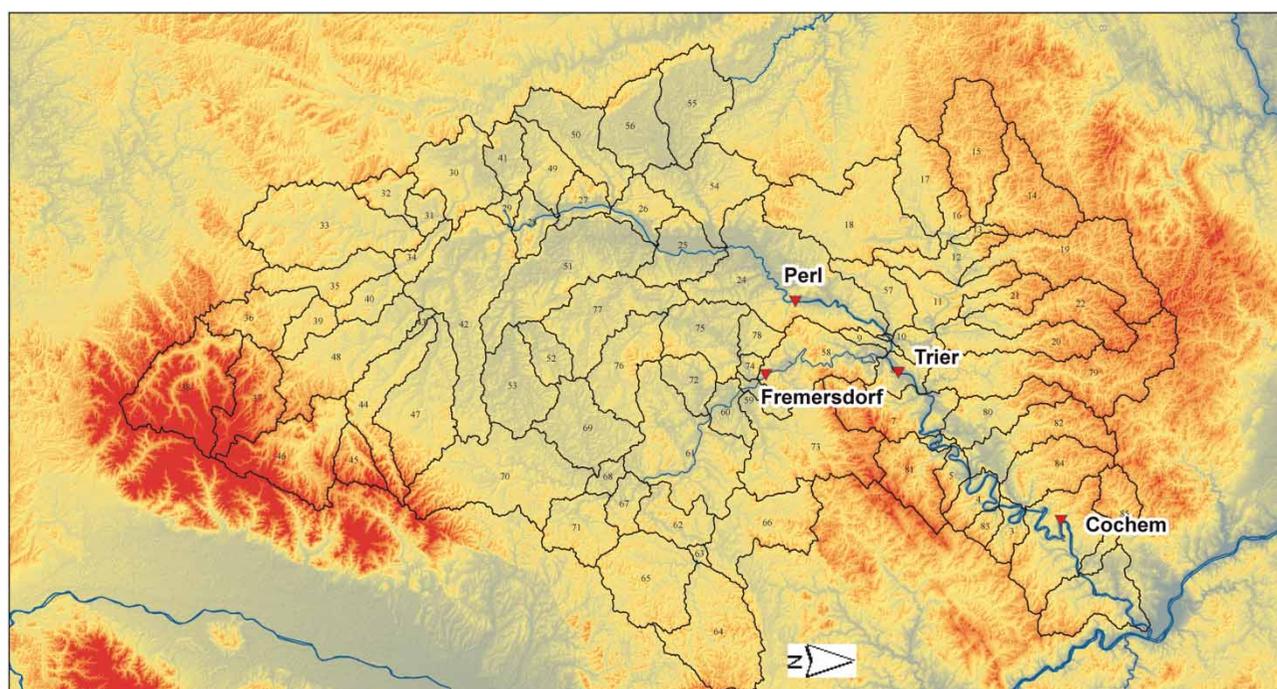

Figure 1 | The Mosel basin including 85 REW modelling elements.

a larger number of stream segments can be used, whereby each link is subdivided into a number of stream segments with a Strahler order lower than a set cut-off order value. By lowering the cut-off value, the amount of segments increases. Here, it is possible to work with a network including 501 segments (cut-off order 3), 951 segments (cut-off order 2) and 1,903 segments (cut-off order 1). We carried out different trials with all four resolution levels and concluded to use 501 reach elements, which proved to be a sound compromise between spatial resolution and computational effort. The bed slopes were extracted from the DEM, whereby in the lower end, bed slopes of the order of 10^{-5} or less were encountered. For numerical reasons, a minimum value of 2.5×10^{-4} was assigned in case the slope was smaller. A uniform Manning coefficient of 0.025 has been assigned to all reaches in conformity with the values used in the operational model currently in use at BFG.

Finally, the channel geometry for the kinematic wave formulation was determined using the Leopold & Maddock (1953) down-stream and at-a-station combined formulation. For the exponents, parameter values from Leopold & Maddock (1953) were employed. For the remaining parameters, values were applied that yielded a channel geometry based on essentially triangular cross sections. Table 1 summarizes the values assumed for the hydraulic geometry.

Table 1 | Leopold & Maddock (1953) scaling coefficients and exponents (Snell & Sivapalan 1995)

At-a-station depth scaling exponent	0.33
At-a-station width scaling exponent	0.33
At-a-station velocity scaling exponent	0.34
Down-stream depth scaling exponent	0.4
Down-stream width scaling exponent	0.5
Down-stream velocity scaling exponent	0.1
Down-stream depth scaling coefficient	0.23
Down-stream width scaling coefficient	7.09
Down-stream velocity scaling coefficient	0.61
Discharge-area scaling coefficient	2.0×10^{-6}
Discharge-area scaling exponent	0.8

SIMULATIONS

We performed flow simulations for the 1 January 1996 to 31 December 2001 period by using hourly forcing to generate lateral inflow time series via the hydrological model. Exactly the same inflows are used for all channel routing simulations. We note that these lateral inflows are generated using uncertain meteorological forcing on the REW model. No data assimilation or input correction has been applied to address the uncertainty in the forcing. The simulated flow is therefore an uncertain and suboptimal estimate of the hourly observed flow. The main purpose of this exercise, however, is to compare the routing methods.

No river–groundwater interaction is assumed to ensure that the amount of water routed through the network is the same for all simulations. The analytical solution (18) is compared against the solution of Equation (6) with the RK method and the solution of the SV equations with SOBEK. Figure 2 provides a schematic view of the interface between the SOBEK and REW models. The stations Perl (Mosel), the inflow point of the Sauer, and Fremersdorf (Saar) were taken as upper model boundaries with concentrated inflows, while lateral inflows further down-stream were distributed uniformly along the main channel of River Mosel. Flow rates were compared at the measurement locations Cochem and Trier. All computations, except SOBEK, were performed in C++ code on a 64 bit LINUX machine cluster.

RESULTS AND DISCUSSION

The results are presented against those obtained with dynamic wave model SOBEK, which we consider as the reference case (SV0) because it involves the numerical solution of the complete SV equation set with the actual surveyed cross-section profiles. All other simulations are compared against the SV0 benchmark case. Table 2 summarizes the characteristics of each simulation run. We note that in the SV0 simulation, all relevant hydraulic structures, such as bridges and weirs, have been modelled. SOBEK performs regular mass balance checks. In case the mass balance error in a computation cell exceeds the order 1×10^{-7}, the code approximates the solution iteratively until the desired error tolerance is reached.
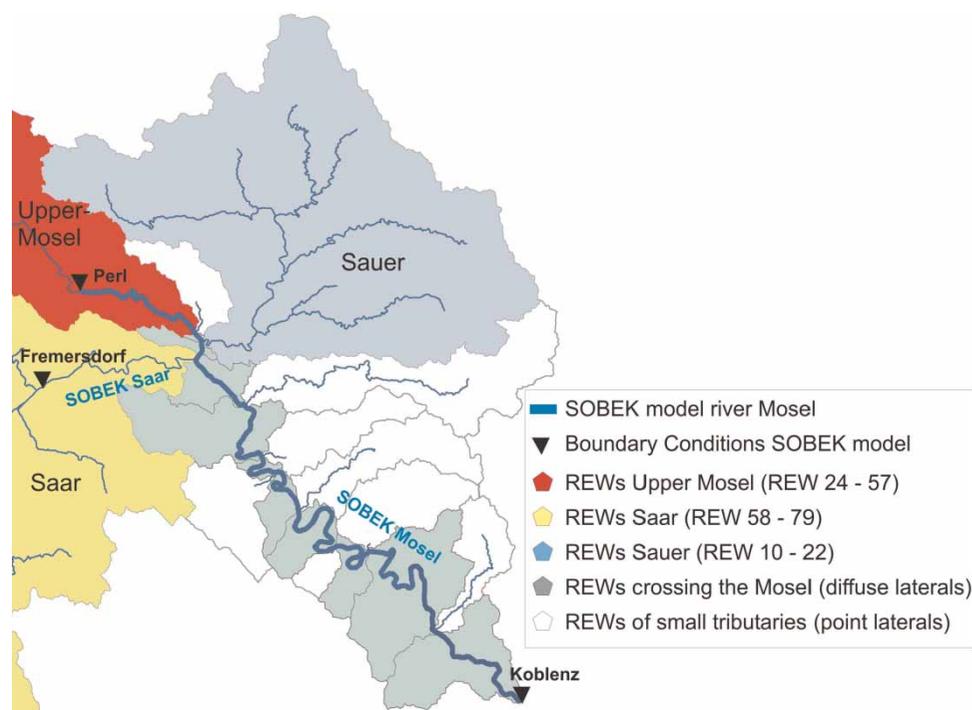
Figure 2 | Coupling of the REW hydrological model and the SOBEK dynamic wave model.

Table 2 | Mass balance and CPU time analysis, Cochem, 1996–2001

Case	Run characteristics	Mass error (m³)	Cumulative outflow volume (mm)	CPU time
Observed	Measured discharge	N/A	2.3272×10^3	N/A
SV0	726 nodes, 3,600 s	$\leq 1.0 \times 10^{-7}$	2.3768×10^3	3 h ca.
AS0	85 elements, $\Delta t = 180$ s	2.6209×10^{-6}	2.4041×10^3	28 min 23 s
AS1	85 elements, $\Delta t = 900$ s	5.0950×10^{-7}	2.4060×10^3	4 min 47 s
AS2	85 elements, $\Delta t = 3,600$ s	7.4340×10^{-7}	2.4031×10^3	1 min 30 s
AS3	501 elements, $\Delta t = 180$ s	2.0209×10^{-6}	2.4031×10^3	29 min 9 s
AS4	501 elements, $\Delta t = 900$ s	1.0437×10^{-6}	2.4031×10^3	5 min 15 s
AS5	501 elements, $\Delta t = 3,600$ s	3.1804×10^{-7}	2.4044×10^3	2 min 28 s
RK0	85 elements, $\varepsilon = 10^{-7}$	4.9813×10^{-7}	2.4004×10^3	23 min 37 s
RK1	85 elements, $\varepsilon = 10^{-5}$	2.5167×10^{-6}	2.4040×10^3	11 min 56 s
RK2	501 elements, $\varepsilon = 10^{-5}$	8.5880×10^{-6}	2.4073×10^3	25 min 19 s

Analytical solution

Six simulations are performed with the analytical solution
(18). In the first case (AS0), we use a network with one
reach element per REW, thus 85 elements in total. The maxi-
mum timestep $\Delta t = 180$ s. In the second (AS1) and third
cases (AS2), we use the same network resolution (85
elements), but increase the timesteps to $\Delta t = 900$ s and
$\Delta t = 3,600$ s, respectively. In doing so, we accept a lower
accuracy of the solution as the local and total truncation
errors increase. Moreover the assumption of constant
inflow and wetted perimeter in Equation (5) breaks down,
leading to progressively larger approximation errors over
longer timesteps due to poorer inflow and wetted perimeter

estimations. In the fourth case (AS3), we increase the number of reach elements to 501, while the timestep $\Delta t = 180$ s. In the fifth (AS4) and sixth cases (AS5), we use 501 elements and $\Delta t = 900$ s and $\Delta t = 3{,}600$ s, respectively. The total mass computation error for all reach elements and the cumulative outflow volume per unit basin area for all cases are summarized in columns three and four of Table 2, while the central processing unit (CPU) times are reported in column five. The CPU times are a good indicator of the relative computational economics of the different solutions, especially as the stepsize for the adaptive timestep method (RK) is controlled by the routing scheme. We note that with the 85 link scheme, an increase of the timestep to $\Delta t = 3{,}600$ s has very little impact on the accuracy of the solution. This is different with the 501 links scheme, where the number of computational cells has been increased by a factor of approximately six. As a result, the model becomes more

sensitive to larger timesteps, whereby the solution starts to deteriorate dramatically for $\Delta t \rightarrow 3{,}600$ s. The approximation error of the solution, mainly caused by the growing local truncation error, is cumulative and therefore has a larger impact on the solution for 501 links with respect to the 85 link case. Figure 3 shows a comparison of the AS0–AS5 solutions against the SV0 reference case and the observed discharge at Cochem for the triple flood peak that occurred between 9 December 1999 and 6 January 2000. Overall, the analytical solutions compare well with the SV0 reference case. We note the slightly higher peaks, which are due to the implicit assumptions of the kinematic wave model to neglect second-order effects, which are responsible for peak attenuation. The consistency with the SV0 case shows (a) the validity of the kinematic wave model for the particular situation, (b) the accuracy of the analytical solution for sufficiently small timesteps (up to 1 h for 85 reach elements)
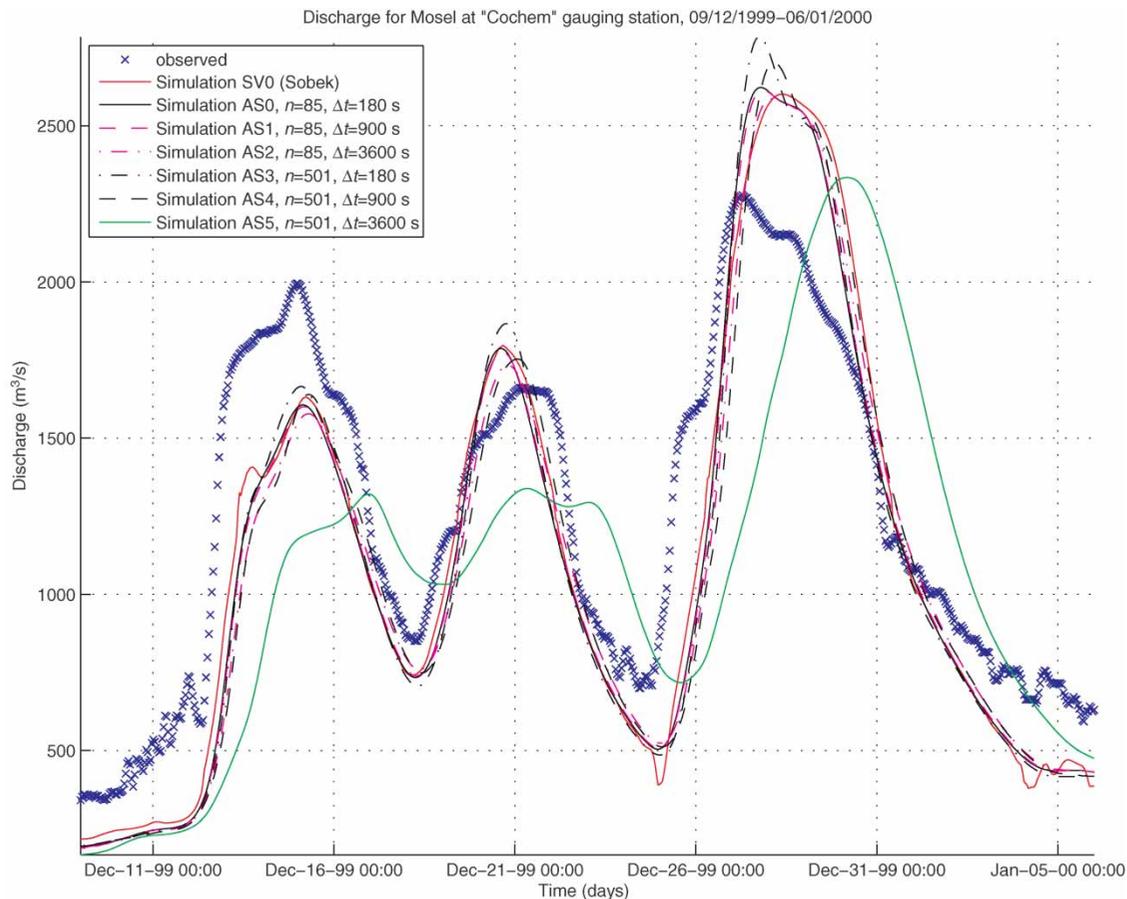

Figure 3 | Inter-comparison of the solutions SV0, AS0–5 and observations for the 9 December 1999 to 6 January 2000 event, Cochem.

and (c) the adequacy of the hydraulic geometry relationships to describe the hydrodynamic properties of the channel.

RK solution

Next, we compare the analytical solution of the kinematic wave with the results obtained by resolving Equation (6) with a fifth-order variable-stepsize RK scheme and examine the sensitivity of method. Three cases were simulated. In the first case (RK0), we use 85 reach elements and an accuracy tolerance $\varepsilon = 10^{-7}$ (see Press *et al.* 2002). The stepsize in this case can drop below 60 s. In the second case (RK1), we accept an accuracy tolerance $\varepsilon = 10^{-5}$, which results in computational efficiency gains by at least a factor two. The results for the 9 December 1999 to 6 January 2000 events are compared in Figure 4. The impact of reducing ε by two orders of magnitude is minimal in terms of cumulative volume

transited at Cochem, as listed in Table 2. In the third case (RK2), the network resolution is increased to 501 links and $\varepsilon = 10^{-5}$. The solutions for the RK0, RK1 and RK2 cases are very similar and barely appreciable to ε. In summary, the RK method performs much worse than the AS0–5 solutions in terms of computation time economics. However, all RK solutions compare well to the SV0 and the AS0–2 solutions during peak and low flows, as visible in Figures 4–6.

SUMMARY AND CONCLUSIONS

We have presented an analytical solution of the kinematic wave equation under a series of assumptions, which are applicable in practical flow routing. The method has been tested by simulating the hydraulics of the River Mosel channel over a 6 year continuous period and compared against
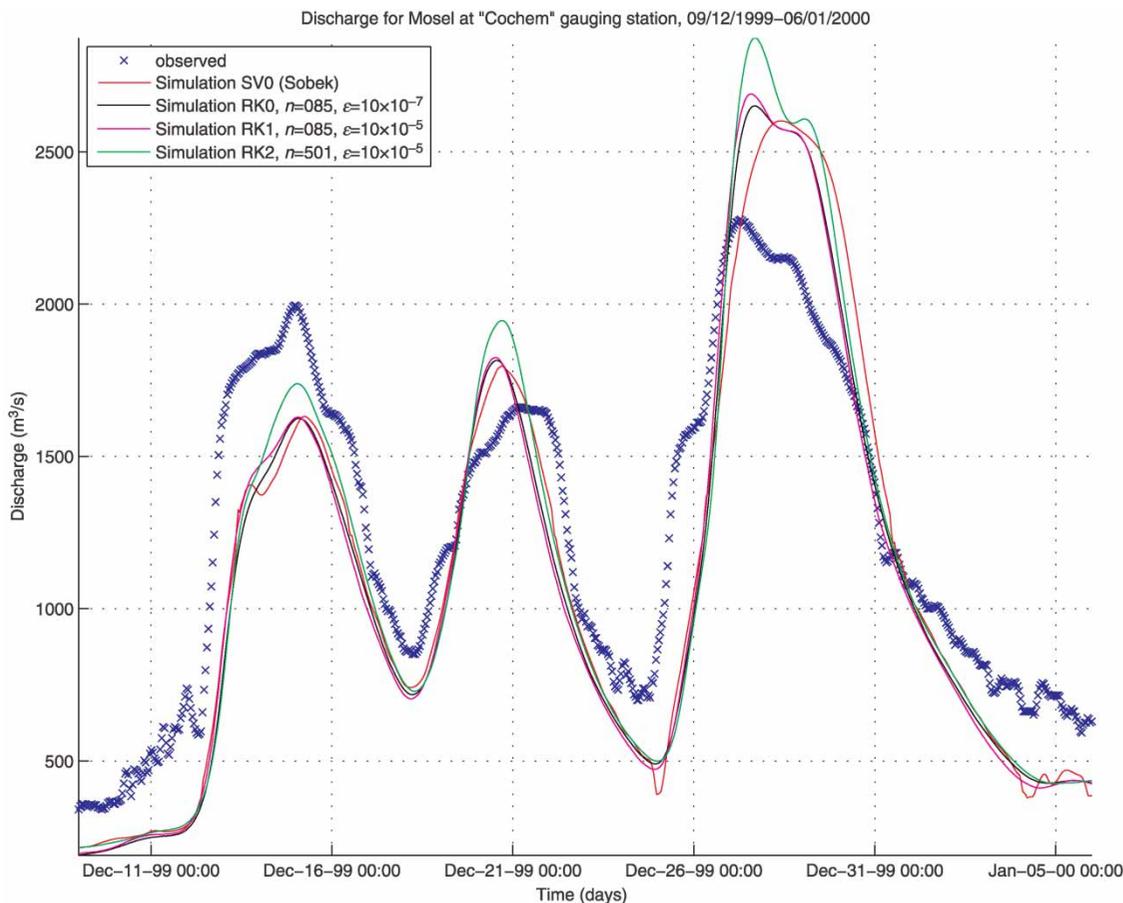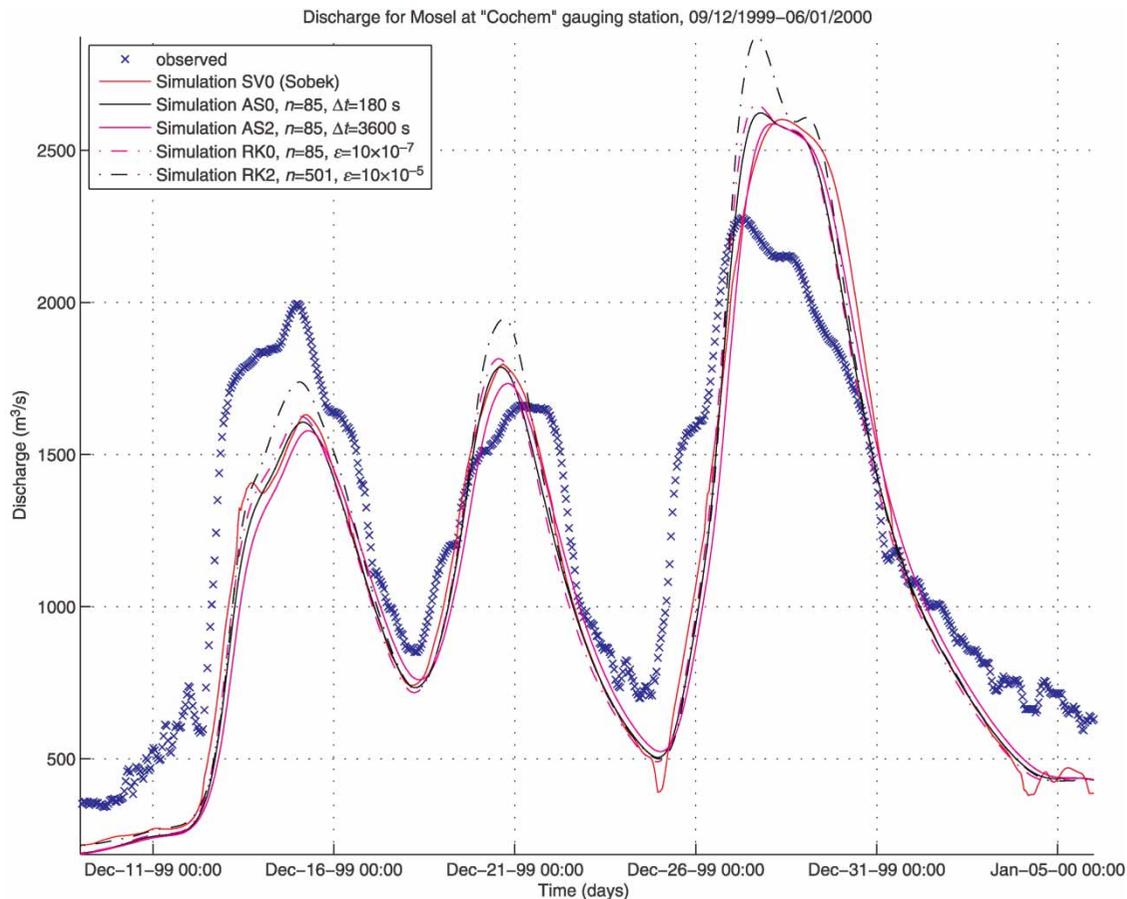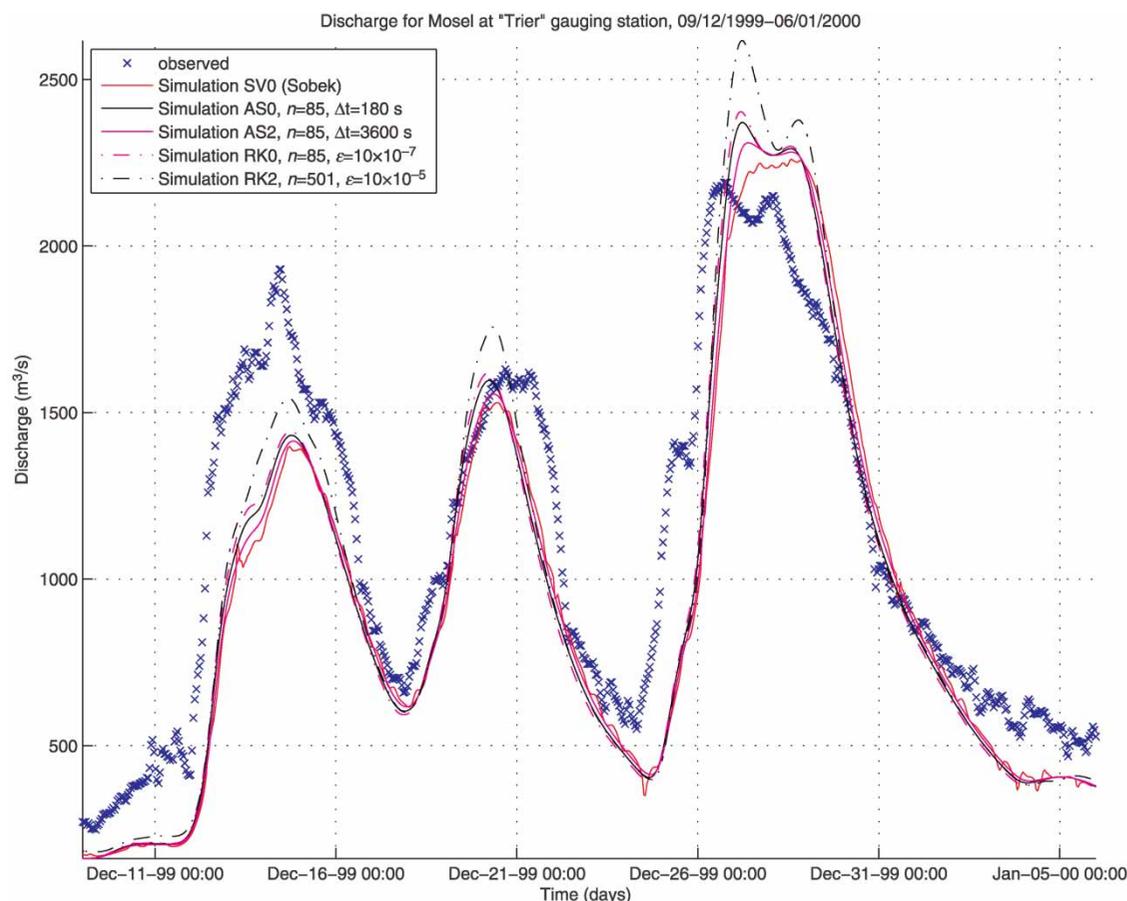

Figure 4 │ Inter-comparison of the solutions SV0, RK0–2 and observations for the 9 December 1999 to 6 January 2000 event, Cochem.

Figure 5 │ Inter-comparison of all solutions and observations for the 9 December 1999 to 6 January 2000 event, Cochem.

the solutions of a complete dynamic wave model and a numerical solution of the original non-linear reservoir equation by using the exact same lateral inflow series for all cases. The findings can be summarized as follows.

- The integral and original form of the non-linear kinematic wave model for a reach element is obtained by combining the mass and energy conservation equations, whereby lateral inflows are assumed constant over a time-step. The result is a non-linear reservoir equation in the form of an ODE.
- We have demonstrated that the analytical solution obtained by means of a second-order Taylor-series approximation of the original equation is third-order accurate, consistent, stable and conservative.
- The utilization of an analytical solution of the kinematic wave equation has a significant advantage in terms of

computational economics with respect to the numerical solution of (i) the ODE with a numerical integrator such as the RK method and (ii) the finite-difference solution of the dynamic wave model.

- It has been shown that the kinematic wave equation in the form of a non-linear reservoir equation can be applied by using empirical relationships to represent the channel geometry. The approach has therefore significant potential to be used for channel routing in ungauged basins, where detailed information on cross-sectional profiles, as required by the dynamic wave model, is unavailable.
- A solution for situations, such as aquifer recharge in which water is lost through the channel bed, has been found that can be used for a whole range of recharge situations potentially encountered in practice.
- The method has been applied to channel routing on River Mosel, and compared against the dynamic wave model

Figure 6 | Inter-comparison of all solutions and observations for the 9 December 1999 to 6 January 2000 event, Trier.

SOBEK. The comparison shows that besides the known inherent limitations of the kinematic wave with respect to the dynamic wave model (absence of the convective acceleration and surface slope terms), the wave solution performs well by requiring a significantly inferior amount of input information.

- On bed slopes that have an order of magnitude equal or larger to 10^{-3}, where peak attenuations are minimal, the kinematic wave model provides an accurate approximation of flood propagation and the solution of the dynamic wave model collapses onto the kinematic wave model.

ACKNOWLEDGEMENTS

REFERENCES

Bergström, S. 1995 The HBV model. In: *Computer Models of Watershed Hydrology* (V. P. Singh, ed.). Water Resources Publications, Highlands Ranch, CO, pp. 443–476.

Chow, V. T. 1968 *Handbook of Hydrology*. McGraw-Hill, New York, NY.

Crawford, N. H. & Linsley, R. K. 1966 Digital simulation in hydrology: Stanford Watershed Model IV, Technical Report No. 39, Stanford University, Palo Alto, CA.

Cunge, J. A. 1969 On the subject of a flood propagation computation method (Muskingum method), Delft, The Netherlands. *J. Hydrol. Res.* **7** (2), 205–230.

Dooge, J. C. I. 1973 Linear Theory of Hydrologic Systems, USDA Technical Bulletin 1468, US Department of Agriculture, Washington, DC.

Henderson, F. M. 1966 *Open Channel Flow*. Macmillan, New York, NY.

Hayami, S. 1951 On the propagation of flood waves, Bulletin no. 1, Disaster Prevention Research Institute, Kyoto University, Japan.

Kalinin, G. P. & Miljukov, P. I. 1957 O raschete neustanovivshegosya dvizheniya vody votkrytykh ruslakh (On the computation of unsteady flow in open channels). *Meteorologiya i Gidrologiya Zhuzurnal, Leningrad* **10**, 10–18 (in Russian).

Kundzewicz, Z. 1985 Hydrodynamic determination of parameters of linear routing models. In: *Scientific Procedures Applied to the Planning, Design and Management of Water Resources Systems* (E. Plate & N. Buras, eds). IAHS, Oxford, IAHS Publication no. 147, pp. 149–160.

Leopold, L. B. & Maddock Jr, T. 1953 The hydraulic geometry of stream channels and some physiographic implications. U.S. Geological Survey Professional Paper 252, US Government Printing Office, Washington, DC.

Lighthill, M. J. & Whitham, G. B. 1955 On kinematic waves. I. Flood movement in long rivers. *Proc. R. Soc. Lond. A* **229**, 281–316.

Liu, Z., Martina, M. L. V. & Todini, E. 2005 Flood forecasting using a fully distributed model: application of the TOPKAPI model to the Upper Xixian catchment. *Hydrol. Earth Syst. Sci.* **9** (4), 347–364.

Liu, Z. & Todini, E. 2002 Towards a comprehensive physically-based rainfall runoff method. *Hydrol. Earth Syst. Sci.* **6** (5), 859–881.

Liu, Z. & Todini, E. 2004 Assessing the TOPKAPI nonlinear reservoir cascade approximation by means of a characteristic lines solution. *Hydrol. Process.* **19** (10), 1983–2006.

McCarthy, G. T. 1940 Flood routing. In: *Flood Control, Chapter V.* Engineer School, Fort Belvoir, VA, pp. 127–147.

Naden, P., Broadhurst, P., Tauveron, N. & Walker, A. 1999 River routing at the continental scale: use of globally available data and an *a-priori* method of parameter estimation. *Hydrol. Earth Syst. Sci.* **3** (1), 109–124.

Nash, J. E. 1957 *The Form of the Instantaneous Unit Hydrograph.* IUGG General Assembly of Toronto, vol. III, IAHS Publication, pp. 114–121.

Ostrowski, M. 1992 A universal module for the simulation of hydrological processes. *Wasser und Boden* **11**, 755–760 (in German).

Ponce, V. M. & Yevjevich, V. 1978 Muskingum–Cunge method with variable parameters. *J. Hydraulic Division, ASCE* **104** (12), 1663–1667.

Press, W. H., Flannery, B. P., Teukolsky, S. A. & Vetterling, W. T. 2002 *Numerical Recipes in C++: The Art of Scientific Computing*, 2nd edn. Cambridge University Press, New York, NY.

Reggiani, P. & Rientjes, T. H. M. 2005 Internal flux parameterisation in the representative elementary watershed (REW) approach: application to a natural basin. *Water Resour. Res.* **41**, W04013.

Reggiani, P., Sivapalan, M. & Hassanizadeh, S. M. 1998 A unifying framework of watershed thermodynamics: balance equations for mass, momentum, energy and entropy and the second law of thermodynamics. *Adv. Water Resour.* **22** (4), 367–398.

Reggiani, P., Sivapalan, M., Hassanizadeh, S. M. & Gray, W. G. 2001 Coupled equations for mass and momentum balance in a stream network: theoretical derivation and computational experiments. *Proc. R. Soc. A* **457**, 157–189.

Snell, J. & Sivapalan, M. 1995 Application of the meta-channel concept: construction of the meta-channel hydraulic geometry for a natural channel. *Hydrol. Proc.* **9**, 485–495.

Stelling, G. S. & Duinmeijer, S. P. A. 2003 A staggered conservative scheme for every Froude number in rapidly varied shallow water flows. *Int. J. Numer. Meth. Fluids* **43**, 1329–1354.

Strupczewski, W. G. & Kundzewicz, Z. W. 1979 Analysis of physical interpretation of parameters of linear conceptual models by means of moment matching method. *J. Hydrol. Sci.* **6**, 143–159.

Tang, X., Knight, D. W. & Samuels, P. G. 1999 Volume conservation in the Variable Parameter Muskingum–Cunge method. *J. Hydraulic Eng. (ASCE)* **125** (6), 610–620.

Todini, E. 2007 A mass conservative and water storage consistent variable parameter Muskingum–Cunge approach. *Hydrol. Earth Syst. Sci.* **11**, 1645–1659.

Todini, E. & Ciarapica, L. 2001 The TOPKAPI model. In: *Mathematical Models of Large Watershed Hydrology* (V. P. Singh & D. K. Frevert, eds), chapter 12. Water Resources Publications, Littleton, CO.

Zhao, R. J. 1992 The Xinanjiang model applied in China. *J. Hyrol.* **135**, 371–381.